Controlled Structure in Artificial Protein Hydrogels

Scott B. Kennedy,*,† Kenneth Littrell,‡ P. Thiyagarajan,‡ David A. Tirrell,§ and Thomas P. Russell†

Department of Polymer Science and Engineering, University of Massachusetts Amherst, Amherst, Massachusetts 01003; IPNS, Argonne National Laboratory, 9700 S. Cass Avenue, Argonne, Illinois 60439; and Division of Chemistry and Chemical Engineering, California Institute of Technology, Pasadena, California 91125

Received April 7, 2005; Revised Manuscript Received June 6, 2005

ABSTRACT: Small-angle X-ray scattering (SAXS) and circular dichroism (CD) were used to study the structure of artificial, multidomain protein hydrogels. Preliminary sedimentation equilibrium results indicate that the flanking leucine zipper domains used in the design of the artificial multidomain protein form tetrameric helical bundles. The leucine zipper domain alone precipitates at high concentrations (7% w/v) and near-neutral pH, but the multidomain protein remains soluble owing to a hydrophilic central domain. The resulting solution displays characteristic properties of physical gels. SAXS data from gels fit well to a cylindrical model with the following dimensions: length 63 Å, radius 13.6 Å, and a 1 Å axial pore. These results match the dimensions of a tetrameric helical bundle and indicate that the low concentration equilibrium structure of the leucine zipper domain is maintained within the multidomain protein, even at high concentrations. Altogether, these results confirm a static picture of the gel structure where tetrameric self-associations of leucine zipper domains act as physical cross-links in the protein hydrogel.

Introduction

Recombinant DNA technology provides a route to the design and synthesis of unique proteins not found in natural systems.[1−6] The foundational design of the protein described herein evolved from two independently studied artificial proteins. One artificial protein, the beta-sheet forming peptide repeat $[(\text{ala-gly})_x\text{-glu-gly}]_y$, fails to demonstrate significant secondary structure in aqueous solutions when an extra proline is present between the (ala-gly) repeat and the glutamic acid residue.[1,3,6] This unstructured peptide sequence, specifically with $X = 3$ and $Y = 10$, shall hereafter be referred to as a random coil domain. Another artificial protein sequence follows the well-studied leucine zipper motif. Leucine zippers fall within a unique class of 7_2-helix forming proteins in that they self-associate under appropriate conditions of pH and temperature. This self-association is intricately tied to the specific sequence of amino acids such that thermal and pH melting transitions, free energies of association, and kinetic strand exchange rates can all be controlled.[7−18] A multidomain protein consisting of two leucine zipper domains flanking a random coil domain could hypothetically form a network structure in solution above the overlap concentration if trimer, or higher order, helical bundles form physical cross-links defined by the leucine zipper interactions. This control over the nature of the physical cross-link, together with recombinant DNA techniques for protein biosynthesis, opens exciting possibilities for engineering gel systems with tailored environmental and physiological response. Furthermore, the central water-soluble domain can also be engineered to include specific functional domains such as sites for targeted enzymatic degradation, cell binding domains, or protein-based therapeutics.

Previous reports by Petka et al. classified these multidomain protein solutions as pH- and temperature-sensitive reversible hydrogels at concentrations above 5% (w/v).[4,19] Initial investigations found correlations between the pH and temperature dependence of the solution state molecular structure of the zipper domains as measured by circular dichroism (CD)[20,21] and the physical properties of gels as measured by diffusing wave spectroscopy (DWS).[22−24] Subsequent NMR studies also suggest that the molecular dynamics of individual leucine zipper domains may correlate with the macroscopic measurements of DWS.[25] While initial results from CD, DWS, and NMR favored hypothetical gel structures wherein leucine zipper interactions dictate cross-link formation, our ultimate objective of engineering artificial protein hydrogels for medical and industrial use demands a more complete description of the gel structure.

Experimental Section

Protein Biosynthesis and Purification. Two proteins were considered for determining gel structure: the single-domain helical protein (**1**) and the multidomain protein (**2**) described and illustrated in Figure 1. Proteins were prepared by expression of the corresponding artificial gene in an *E. coli* host, strain SG13009 containing the repressor plasmid pREP4 (Qiagen, Chatsworth, CA). Construction of the artificial genes in the expression plasmid pQE9 (Qiagen) has been previously reported.[18] The pQE9 expression plasmid encodes an NH_2-terminal hexahistidine sequence that facilitates protein purification by immobilized metal affinity chromatography.

Small cultures (5 mL) of the expression strains were inoculated from frozen stocks in 2xYT media (16 g of casein hydrolysate, 10 g of yeast extract, and 5 g of NaCl per liter of culture). After incubation at 37 °C for 5−6 h, 25 μL aliquots were used to inoculate larger cultures (25 mL) in 2xYT media, which incubated at 37 °C overnight. The 25 mL cultures were

† University of Massachusetts Amherst.
‡ Argonne National Laboratory.
§ California Institute of Technology.
* To whom correspondence should be addressed. Current address: Eastern Mennonite University, 1200 Park Road, Harrisonburg, VA 22802. E-mail: scott.kennedy@emu.edu.

10.1021/ma050726l CCC: $30.25
Published on Web 07/21/2005

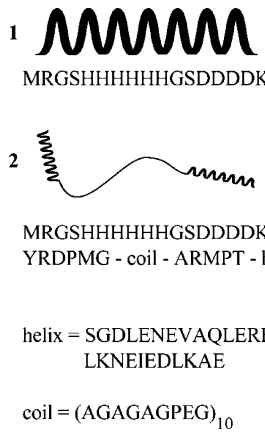

Figure 1. Schematic illustrations and amino acid sequences of proteins **1** and **2** investigated herein. The six histidine units at the N-termini of each protein allow for protein purification by metal affinity chromatography. Other amino acid units not defined within the helix or coil domains are linker regions that are a byproduct of the recombinant DNA strategy for protein biosynthesis.

then used, in their entirety, to inoculate 12 L cultures in 1xLB media (10 g of casein hydrolysate, 5 g of yeast extract, 10 g of NaCl, and 40 mg of NaOH per liter of culture). All media were supplemented with ampicillin (100 mg/L) and kanamycin (25 mg/L). Once inoculated, 12 L cultures were incubated at 37 °C until optical densities (600 nm, OD_{600}) reached one. At $OD_{600} > 1$, protein expression was induced by addition of isopropyl-β-thiogalactoside (1 mM). After 4 h, the cell culture was sedimented by centrifugation at 4 °C, 15000*g* for 10 min. Cell pellets were washed, then resuspended in sonication buffer (50 mM NaH_2PO_4, 300 mM NaCl, 10 mM imidazole, pH 8), and frozen at −20 °C.

Cells were lysed first by thawing and then by sonication. After centrifugation for 20 min at 4 °C, 15000*g* to remove insoluble cellular matter, the supernatant was collected for purification. Target proteins were isolated from the supernatant by affinity chromatography on a nickel−nitrilotriacetic acid resin (Ni^{2+}−NTA, Qiagen) following the native purification protocol provided by Qiagen. Column fractions containing pure protein in elution buffer (50 mM NaH_2PO_4, 300 mM NaCl, 250 mM imidazole, pH 8) were collected and dialyzed under continuously refreshed DI water for 3−4 days and then lyophilized. Yields for **1** and **2** were 100 ± 20 mg of protein per liter of culture.

Further purification was achieved by reverse phase high-pressure liquid chromatography (HPLC) for preparing CD and ultracentrifugation samples. HPLC was performed on a Waters system comprised of a 717plus autosampler, a 486 tunable absorbance detector, and a 600 controller equipped with a Nova-Pak C_{18} 3.9 × 150 mm column. Proteins were dissolved in 200 mM Tris buffer, pH 7.4, and filtered before injection. Elution profiles were collected at a flow rate of 1 mL/min and monitored at 214 nm. The mobile phase was a linear gradient mixture of water to acetonitrile run over a period of 60 min. Both solvents contained 0.1% (v/v) trifluoroacetic acid (TFA) and were degassed with helium. Eluent fractions containing pure protein were collected and freeze-dried.

Circular Dichroism. CD samples were prepared from a 1 mg/mL stock solution of HPLC purified **2** in DI water. Final sample conditions were 5 μM protein, 10 mM NaH_2PO_4, and 150 mM NaCl. Sample pH was adjusted using 8 N NaOH or 1 N HCl, as appropriate. CD data were recorded on a Jasco J-715 spectropolarimeter using the following run conditions: 1.0 mm path length rectangular quartz cell (Hellma), 1.0 nm bandwidth, 2 s response, 20 mdeg sensitivity, and constant N_2 flushing. Thermal melting profiles were collected by monitoring the CD signal at 222 nm ($[\theta]_{222}$) as a function of temperature using a Jasco PTC-348W1 thermostatically controlled cuvette holder. Signal was recorded every 0.1 °C as the sample temperature was ramped at a rate of 1 °C/min. Both heating and cooling ramps were run in order to observe any hysteresis.

Assuming a two state model to describe the equilibrium between folded and unfolded states, thermal melting profiles were fit to eq 1

$$\theta = \theta_f + m_f T + (\theta_u + m_u T - \theta_f - m_f T)[e^{-\Delta H/RT+\Delta S/R}/(1 + e^{-\Delta H/RT+\Delta S/R})] \quad (1)$$

where T is the temperature in kelvin, θ is the CD signal at 222 nm, θ_f and θ_u are the values of the CD signal for the folded and unfolded peptide, respectively, extrapolated linearly to 0 K, and m_f and m_u are the respective slopes of the linear extrapolation.[26] The inflection point of the curve represents the temperature at which half the leucine zipper domains are folded and half are unfolded.

Analytical Ultracentrifugation. Samples for ultracentrifugation were prepared from 10 mg/mL stock solutions of HPLC purified **1** and **2** in 200 mM Tris buffer, pH 7.4, and 150 mM NaCl. Sedimentation equilibrium profiles were collected using a Beckman Optima Series analytical ultracentrifuge equipped with an An-60 Ti analytical rotor and cells. Samples were equilibrated at 20 °C and a rotor speed of 22000 rpm for 2−3 days. Equilibrium was verified by the overlapping of one profile with another collected 10 h later. Once equilibrated, 15 scans were taken and compiled for analysis. The ultracentrifuge was equipped with XL-I integrated optics and XL-A absorbance capabilities for both refractive index (RI) and ultraviolet (UV) absorbance detection of concentration gradients. Both detection techniques were utilized; UV absorbance measurements were performed at 280 nm. At high concentrations (10, 7.5, 5.0, and 2.5 mg/mL), Beer's law is inapplicable, and UV data from these samples were not analyzed. Ultracentrifugation data were analyzed using *WinNonlin V1.035 Nonlinear Least Squares Fit Program For Equilibrium Ultracentrifuge Analysis* obtained from the Web page of The National Analytical Ultracentrifugation Facility of the University of Connecticut Biotechnology Center (http://www.ucc.uconn.edu/~wwwbiotc/UAF.HTML).

Small-Angle X-ray Scattering. Gels for SAXS were prepared by dissolving 70 mg of **2** in 1 mL of buffer (100 mM Tris, 100 mM 2-amino-2-methyl-1-propanol, pH not adjusted prior to protein dissolution). Upon dissolution of protein, a pH of 4.9 was measured. An 8 N NaOH solution was added incrementally to adjust pH. Several aliquots were transferred to 1 mm quartz capillaries (Charles Supper Co.) at each of the following values of pH: 4.9, 6.5, 7.2, 7.6, 7.9, 8.3, 8.8, 9.4, and 12+. For each pH, two scattering profiles were collected: nonannealed samples (still fluid) and samples annealed at 80 °C for 2 min and then quenched to room temperature (gels). Temperature-dependent scattering profiles were also taken for six annealed samples (pH 4.9, 6.5, 7.2, 8.3, 9.4, and 12+). Samples were heated from 25 to 80 °C at a rate of 2 °C/min using a Linkam TMS 93 temperature controller and THMS 600 hot stage mounted in the beam. Temperature-dependent data were collected at one exposure per minute.

SAXS was performed on the high brilliance undulator beamline (ID-12, BESSRC-CAT) at the Advanced Photon Source (APS), Argonne National Laboratory.[27] Scattered X-rays were detected using a 15 cm × 15 cm, 9-segment, 2-dimensional CCD gold detector. Three sample-to-detector distances (4, 2, and 1 m) were used with beam energies of 12 and 10 keV. These instrument configurations allowed the magnitude of the scattering vector, $q = (4\pi/\lambda) \sin \theta$, to be explored between 0.005 and 0.7 Å^{-1} where 2θ represents the scattering angle and λ represents the wavelength of the X-rays. Data were corrected for dark current and image distortion then azimuthally averaged. Background scattering profiles were collected from buffer solutions and treated identically. Background scattering was subtracted from experimental data in 1-dimensional format, and the resulting profiles were analyzed using macros developed within the framework of Igor Pro software.

Exposure times required for good statistics were 1 s at the 4 m configuration and 0.2 s at the 2 and 1 m configurations. Room temperature experiments consisted of five exposures with a 1 s delay between exposures. For the temperature-dependent experiments, one exposure was taken per minute over the time course of heating. We also performed an initial series of experiments to determine the total exposure time (dose) that would damage the sample. Although radiation damage was never quantified, our use of a Tris buffer and limiting doses (total exposure time) kept radiation damage at a minimum. All exposures were, at most, one-fifth the dose where observable damage occurred. Furthermore, individual capillary samples were never used for more than one experiment to minimize effects of radiation damage.

Computer Model for Theoretical Scattering. The exact equation for the form factor of a cylinder cannot be solved analytically; hence, most solutions rest on the assumption that the axial dimension of the cylinder is much larger than the diameter. Unfortunately, this assumption is not necessarily valid for the helical bundles expected in the gel structure. For this reason, a simple Monte Carlo computer simulation was written to generate theoretical scattering profiles from compact cylinders. The simulation was based on a general, hollow cylinder model with the following input parameters: R_i (inner radius), R_o (outer radius), L (length), N (number of scatterers), q_{min}, and q_{max}. Point scatterers were randomly placed to fill the model space, and the theoretical scattering profile was calculated according to eq 2.

$$S(q) = \frac{1}{N^2}\sum_i\sum_j \frac{\sin(qr_{ij})}{qr_{ij}} \tag{2}$$

The variable r_{ij} represents the distance between the ith and jth scatterers. Theoretical scattering profiles from helical bundles were simulated on the basis of dimensions of length and radius reported in the literature for other leucine zipper systems.[28−31] Most simulations were run with $R_i = 0$ Å, although one tetramer bundle simulation was run with $R_i = 5$ Å. The number of point scatterers (N) was chosen to be proportional to the number of electrons in each bundle. If N were set equal to the total number of electrons in a helical bundle, the calculations would require an unreasonable amount of time. Hence, N was set such that each bond and each atom was treated as a point scatterer.

Results and Discussion

Dilute Solution Structure. The task of elucidating gel structure began with dilute solution CD of two proteins nearly identical to **1** and **2** with the exception that each contains a C-terminal cysteine residue. Subsequently, efforts shifted to studying **2** to avoid potential difficulties arising from the effects of disulfide bonding at the C-terminus. Figure 2 compares the thermal melting of **2** with data previously reported for the cysteine terminal analogue.[4,19] The proteins behave similarly, although **2** exhibits a slightly lower transition temperature than the cysteine-terminal analogue between pH 7 and pH 9.5. This observation is consistent with a report by Hodges et al. where it was shown that an S−S link at the N-terminus of a similar leucine zipper peptide raises the temperature of the melting transition by 6.5 °C.[32] Neither **2** nor the cysteine terminal analogue exhibits any measurable thermal transitions below pH 6. These results, along with data reported by Petka et al. describing the melting transition of the isolated leucine zipper domain, indicate that leucine zipper interactions control the thermal behavior of **2** in dilute solution. Hence, if leucine zipper structures in concentrated gels and dilute solutions exhibit similar pH and thermal dependence, the evidence for molecular control of macroscopic physical properties strengthens.

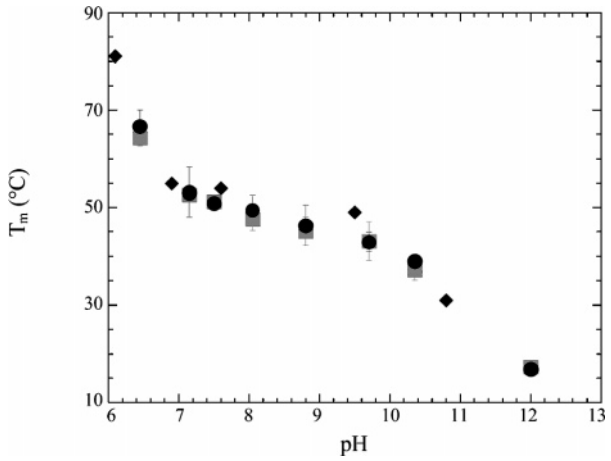

Figure 2. Thermal melting transitions for **2** (5 μM) measured by CD under conditions of increasing (●) and decreasing (■) temperature. Data reported by Petka et al.[18] for a cystiene terminal analogue of **2** (5 μM) are also plotted for comparison (◆).

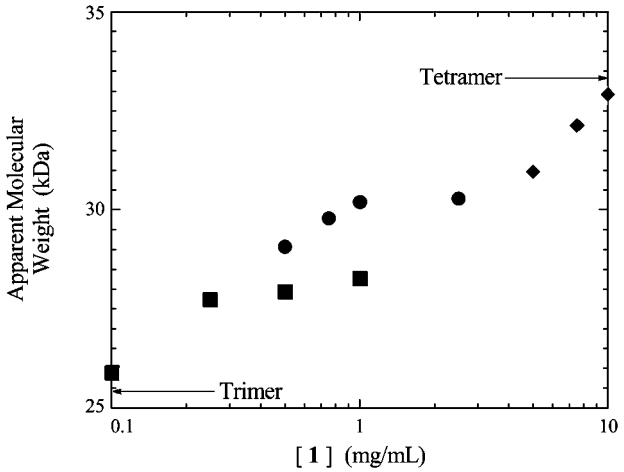

Figure 3. Summary of apparent molecular weights determined by analytical ultracentrifugation of **1**. Both RI (●, ◆) and UV (■) detection were utilized to measure concentration. Fits to data at the three highest concentrations (◆) are poor and indicate nonideal associations. Expected molecular weights for trimer and tetramer bundles are shown as a visual aid.

While CD verifies the existence of temperature- and pH-dependent structures in dilute solution, the experiments provide no information pertaining to the state of association of the helical domains in question. Preliminary results from analytical ultracentrifugation provide evidence that the leucine zipper domains form tetrameric helical bundles. These results are preliminary because they only attempt to approximate the apparent molar mass of the helical bundles, thus providing a glimpse of the equilibrium state of association and a static picture of a possible gel structure. A second paper is envisioned that would combine fluorescence exchange experiments with an exhaustive series of analytical ultracentrifugation experiments to elucidate the dynamic nature of the equilibrium between self-associating domains and the dynamic nature of the gel structure.

Figure 3 summarizes results from the preliminary set of analytical ultracentrifugation experiments. The ap-

parent MW from the fits varied with concentration but also depended on whether RI or UV detection was used. The range of concentrations investigated required using both detection techniques; hence both are shown. Results verify that **1**, the zipper domain alone, self-associates into bundles larger than three helices per bundle since the apparent molecular weight is larger than that of a trimer at all concentrations. Furthermore, the data appear to approach the expected molecular weight of a tetramer, although the highest concentration data remain suspect. Residuals of the high concentration fits indicate nonideal associative behavior, which is consistent with the visual observation of precipitate formation and explains the nonasymptotic approach toward an equilibrium molecular weight. Nonetheless, the data in Figure 3 indicate that a tetrameric helical bundle is likely the predominant equilibrium structure of **1** at concentrations between 1 and 10 mg/mL (about 0.1−1 mM). The onset of precipitation within this concentration range prohibits direct investigation of **1** at concentrations above 1 mM. To probe the structure of the helical bundles at higher concentrations, a water-soluble domain must be present to prevent precipitation. Such is the case with the multidomain protein, **2**, which forms gels at concentrations above 2 mM (or a total helical domain concentration above 4 mM).

Analytical ultracentrifugation of a dilute solution of **2** further confirmed the presence of tetrameric helical bundles, but data from higher concentrations proved difficult to analyze. Certain steps could be taken to further investigate higher concentrations and certain gel properties of **2** by analytical ultracentrifugation. SAXS, however, provided a more direct means to investigate the gel structure, specifically the leucine zipper aggregates.

Concentrated Solution Structure. Analysis of SAXS data initially approaches the system by modeling helical bundles as cylindrical scatterers. Several X-ray diffraction studies from the leucine zipper literature support this first approximation and provide guidance for SAXS analysis.[11,28−31] Equation 3 completely describes the amplitude (F_1) scattered from a cylinder with cross section A and length L.[33]

$$F_1(\bar{q}) = (\Delta\rho)L\,\frac{\sin\left(\frac{qL\gamma}{2}\right)}{\frac{qL\gamma}{2}}\int\int \mathrm{d}A\; \mathrm{e}^{-i\bar{q}\bar{r}_c} \qquad (3)$$

In this and subsequent equations, $\Delta\rho$ represents the difference in electron density between the cylinder and the surrounding medium, $\bar{q}$ represents the scattering vector with magnitude q, γ represents the cosine of the angle between $\bar{q}$ and the cylinder axis, and $\bar{r}_c$ represents the radial vector in the plane of the cylinder cross section. Terms inside the integral represent contributions to scattering from the cross section of the cylinder. Factors outside the integral represent scattering contributions from the axial component. The total scattered intensity from this system equals the square of $F_1(\bar{q})$ averaged over all orientations. Unfortunately, an exact solution to this ensemble average is not available, and any general solution requires certain approximations.

A common approximation for cylindrical systems at intermediate q requires that $L \gg d$, where d represents the cylinder diameter. In such cases the axial and cross-sectional components of the system effectively scatter independently. As such, eq 3 conveniently splits into two separate equations, each averaged independently over all orientations. The two solutions combine to give eq 4, an approximation for the scattered intensity from a cylinder.

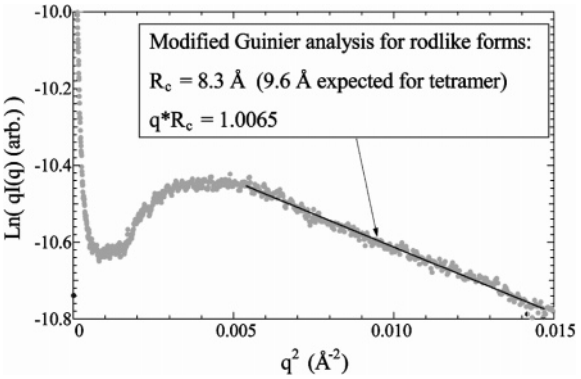

Figure 4. A representative plot for the modified Guinier analysis of SAXS collected from gels. The slope of the linear region between 0.005 and 0.015 Å^{-2} provides the cross-sectional radius of gyration for a cylindrical scatterer. This particular data were collected from a 7% (w/v) gel of protein **2** at pH 7.6 and 25 °C.

$$I(q) = \frac{\pi}{q}(\Delta\rho)^2 LA^2 \mathrm{e}^{-q^2R_c^2/2} \qquad (4)$$

In eq 4, referred to as a modified Guinier analysis for a rod, R_c represents the cross-sectional radius of gyration of the cylinder. Thus, plotting $\ln[I(q)q]$ as a function of q^2 should yield a straight line with a slope of $R_c^2/2$ from which the radius R can be determined using $R = R_c\sqrt{2}$.

As a first approximation, the scattering from gels should resemble the scattering from a dilute solution of helical bundles. This approximation should hold because the helical domains and their associated states comprise only about 2% of the total volume of the system and exhibit a higher electron density than the unstructured random coil domain and the solvent. Thus, the scattering from helical domains should dominate the overall scattering, especially at low q. Figure 4 shows a typical modified Guinier plot for a rod of the scattering from gels comprised of protein **2**. The bend over of the curve where $q^2 < 0.004$ Å^{-2} can be due either to the interparticle correlations of the rods or to the finite length of the bundles at which length scale the correlation of the single rod breaks down. In either case the derived R_c from the SAXS data should be reliable. The slope of the data at $qR_c \leq 1$ yields a value of $R_c = 8.3$ Å (R = 11.7 Å). This value is a little lower than the reported values around 9.6 Å (R around 13.6 Å) for other tetrameric leucine zippers.[11,30] The discrepancy may be due to molecular packing in the self-assembly.

To get a better understanding of the structure of the rodlike regions, scattering profiles were simulated and compared with theory incorporating a more general form factor. Recent X-ray diffraction studies on tetrameric helical bundles suggest the presence of a 1 Å pore in the interstitial region of the helices.[11] Figure 5 shows the consistency between experimental data and a simulated scattering profile that includes a 1 Å pore in the model. This is a compelling argument for the presence of tetrameric helical bundles in gels near physiological pH.

Figure 6 shows the effect of pH on R_c. Near physiological pH, R_c appears unaffected by annealing and is

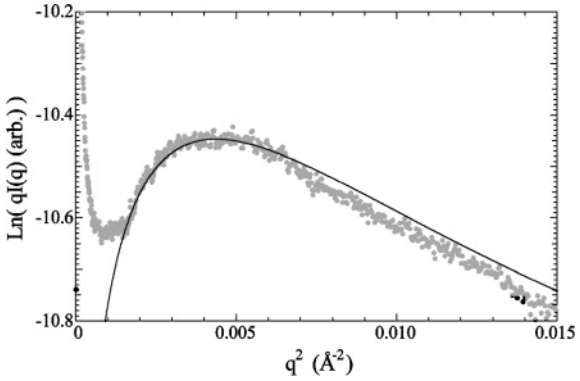

Figure 5. Data from Figure 4 plotted with simulated data (solid line) from a model for tetrameric bundles with a 1 Å pore.

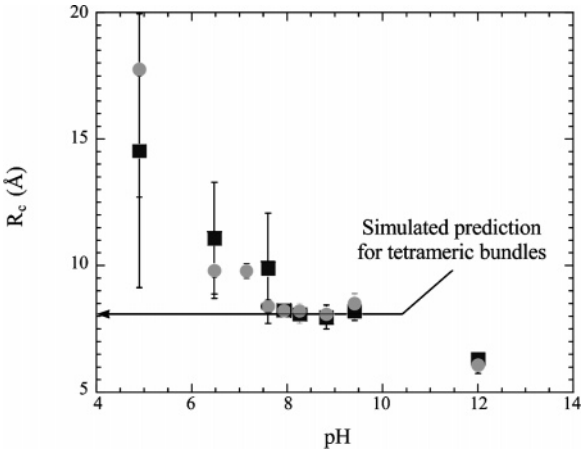

Figure 6. Cross-section radius of gyration for 7% (w/v) solutions of protein **2** at different pH before (■) and after (●) a 2 min anneal at 80 °C.

consistent with the expected R_c of a tetramer. Furthermore, other observations explain deviations from the expected R_c at high and low pH. At high pH, CD indicates that nearly 100% of helical structures have unfolded at 25 °C, hence the dramatic reductions in R_c. At low pH, specifically pH 4.9 and 6.5, the error bars in Figure 6 indicate that the size distribution of bundles widens as pH decreases. Modified Guinier analysis of the SAXS data for samples at low pH showed profiles with two distinct regions and a slight upward curvature at intermediate q. This likely arises from further associations of bundles and is consistent with several observations indicating increased thermal stability at low pH. First, CD reveals a stabilization of helical structures, as nearly 100% of helical structures remain at pH 5.35 and a temperature as high as 90 °C. Second, analytical ultracentrifugation suggests nonideal helical associations occur at very high concentrations, even at physiological pH. Finally, extended annealing of samples at high concentration and low pH *does* lead to precipitation.

Evidence that helical bundles within the gel structure also exhibit similar temperature dependence to those in dilute solution would further validate the hypothesis that the molecular design of the leucine zipper domains controls the macroscopic properties of the gel. Temperature-dependent SAXS provides this evidence. Figure 7 shows the temperature dependence of R_c for four samples at different pH. At each pH the onset of structural changes, as measured by SAXS, occurs at a temperatures higher than the thermal unfolding transitions reported in Figure 2. This discrepancy could arise from the inherent difference between the two experimental techniques or from concentration effects.

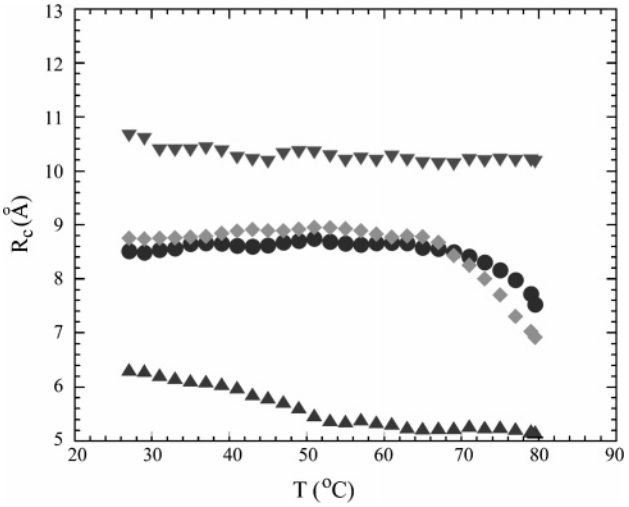

Figure 7. Temperature dependence of R_c plotted for 7% (w/v) gels of protein **2** at four different pH: 6.5 (▼), 8.3 (●), 9.4 (◆), and 12 (▲).

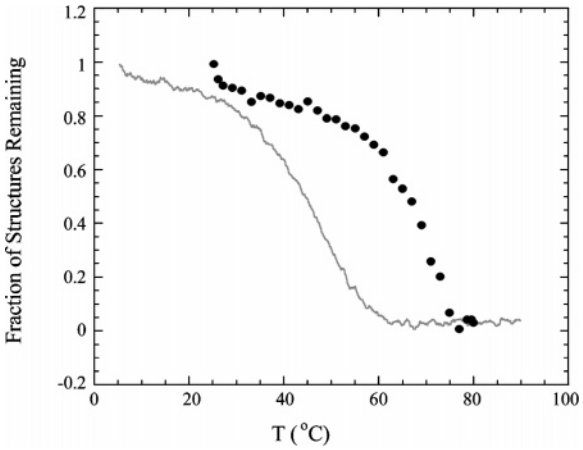

Figure 8. Comparing protein **2** structural information obtained from CD (—) and SAXS (●) at pH 8.1 and pH 8.3, respectively. The CD signal at 222 nm was normalized between θ_f and θ_u to determine the fraction of helical structures remaining. The SAXS signal at $q = 0.063$ Å was normalized between the highest and lowest measured intensities to approximate the fraction of helical structures remaining.

By definition, the thermal unfolding temperature measured by CD indicates the temperature at which half of the helical structures remain. The angular dependence of the SAXS, on the other hand, measures the time-averaged structure in the system but cannot provide a quantitative measure of structures remaining. In addition, the measured R_c represents a z-averaged value. Consequently, significant changes in the size distribution of helical bundles must occur before any changes are observed in the angular dependence of the SAXS. A better comparison between SAXS and CD would follow from the temperature dependence of the SAXS intensity because the scattered intensity is proportional to the number of scattering elements. Figure 8 shows that the SAXS intensity at a fixed q, just before the bend over region in a modified Guinier analysis, decreases with increasing temperature and compares this with CD data. Both sets of data are normalized between their respective signal intensities at the low- and high-temperature asymptotes. This normalization

strategy provides a quantitative interpretation of CD data because the signal intensity is proportional only to the total helical content in the system. The signal intensity from SAXS, however, is proportional to the number of scattering elements (helical bundles) as well as other electron density fluctuations with similar correlation lengths. These minor contributors to the scattered intensity may slightly change with temperature, so Figure 8 only provides a semiquantitative interpretation of the SAXS data.

A conservative estimate of thermal unfolding temperatures derived from Figure 8 suggests an increase of 25 °C between dilute solution and concentrated gel. This is consistent with the hypothesis that the stability of leucine zipper associations increases with increasing protein concentration. Thermal unfolding temperatures in similar leucine zipper systems have been reported to span a 20 °C temperature range over concentrations between micromolar and millimolar levels.[13,16] Thus, the difference between thermal unfolding temperatures measured from the SAXS sample (3 mM solution) and the CD sample (5 μM solution) is not unexpected.

Conclusions

Results from circular dichroism, analytical ultracentrifugation, and small-angle X-ray scattering all point to a network structure in concentrated solutions of protein **2** consisting of leucine zipper tetrameric bundles acting as physical cross-links. Near physiological pH, the helical bundles appear stable in their equilibrium tetrameric state, even though the helical domains themselves would precipitate at the concentrations necessary for gelation. The water-soluble, random coil domain appears to prevent the helical bundles from precipitating. Even so, the helical bundles exhibit similar structural thermal and pH dependence both in the gel and in dilute solutions.

Acknowledgment. This work was supported by the Materials Research Science and Engineering Center at the University of Massachusetts Amherst (DMR-9809365). The authors thank Paul Welch for assistance in the modeling and simulation of SAXS data and Soenke Seifert in the SAXS measurements. This work benefited from the use of BESSRC-CAT at APS and IPNS, funded by the U.S. DOE, BES under Contract W-31-109-ENG-38 to the University of Chicago.

References and Notes

(1) Creel, H. S.; Fournier, M. J.; Mason, T. L.; Tirrell, D. A. *Macromolecules* **1991**, *24*, 1213−1214.
(2) Krejchi, M. T.; Atkins, E. D. T.; Waddon, A. J.; Fournier, M. J.; Mason, T. L.; Tirrell, D. A. *Science* **1994**, *265*, 1427−1431.
(3) Parkhe, A. D.; Fournier, M. J.; Mason, T. L.; Tirrell, D. A. *Macromolecules* **1993**, *26*, 6691−6693.
(4) Petka, W. A.; Harden, J. L.; McGrath, K. P.; Wirtz, D.; Tirrell, D. A. *Science* **1998**, *281*, 389−392.
(5) Tirrell, D. A.; Fournier, M. J.; Mason, T. L. *MRS Bull.* **1991**, 23−28.
(6) McGrath, K. P.; Fournier, M. J.; Mason, T. L.; Tirrell, D. A. *J. Am. Chem. Soc.* **1992**, *114*, 727−733.
(7) McGrath, K. P.; Kaplan, D. L. *Mater. Res. Soc. Symp. Proc.* **1993**, *292*, 83.
(8) Cohen, C.; Parry, D. A. D. *Proteins Struct. Funct. Genet.* **1990**, *7*, 1−15.
(9) Hodges, R. S. *Biochem. Cell Biol.* **1996**, *74*, 133−154.
(10) Monera, O. D.; Zhou, N. E.; Lavigne, P.; Kay, C. M.; Hodges, R. S. *J. Biol. Chem.* **1996**, *271*, 3995−4001.
(11) Harbury, P. B.; Zhang, T.; Kim, P. S.; Alber, T. *Science* **1993**, *262*, 1401−1406.
(12) Zhou, N. E.; Kay, C. M.; Hodges, R. S. *J. Biol. Chem.* **1992**, *267*, 2664−2670.
(13) Lumb, K. J.; Kim, P. S. *Science* **1995**, *268*, 436−438.
(14) Porte, D.; Oertel-Buchheit, P.; Granger, S.; Michele; Schnarr, M. *J. Biol. Chem.* **1995**, *270*, 22721−22730.
(15) Zhou, N. E.; Kay, C. M.; Hodges, R. M. *Proein Eng.* **1994**, *7*, 1365−1372.
(16) Durr, E.; Jelesarov, I.; Bosshard, H. R. *Biochemistry* **1999**, *38*, 870−880.
(17) Wendt, H.; Berger, C.; Baici, A.; Thomas, R. M.; Bosshard, H. R. *Biochemistry* **1995**, *34*, 4097−4107.
(18) Zhou, N. E.; Zhu, B.-Y.; Kay, C. M.; Hodges, R. S. *Biopolymers* **1992**, *32*, 419−426.
(19) Petka, W. A. *Reversible Gelation of Genetically Engineered Macromolecules*; University of Massachusetts: Amherst, 1997.
(20) Fasman, G. D. *Circular Dichroism and the Conformational Analysis of Biomolecules*; Plenum Press: New York, 1996.
(21) Chen, Y.-H.; Yang, J. T.; Chau, K. H. *Biochemistry* **1974**, *13*, 3350−3359.
(22) Durian, D. J.; Weitz, D. A.; Pine, D. J. *Science* **1991**, *252*, 686−688.
(23) Pine, D. J.; Weitz, D. A.; Chaikin, P. M.; Herbolzheimer, E. *Phys. Rev. Lett.* **1988**, *60*, 1134−1137.
(24) Weitz, D. A.; Zhu, J. X.; Durian, D. J.; Gang, H.; Pine, D. J. *Phys. Scr.* **1993**, *T49*, 610−621.
(25) Kennedy, S. B.; deAzevedo, E. R.; Petka, W. A.; Russell, T. P.; Tirrell, D. A.; Hong, M. *Macromolecules* **2001**, *34*, 8675−8685.
(26) O'Shea, E. K.; Rutkowski, R.; Kim, P. S. *Cell* **1992**, *68*, 699−708.
(27) Seifert, S.; Winans, R. E.; Tiede, D. M.; Thiyagarajan, P. *J. Appl. Crystallogr.* **2000**, *33*, 782−784.
(28) Rasmussen, R.; Benvegnu, D.; O'Shea, E. K.; Kim, P. S.; Alber, T. *Proc. Natl. Acad. Sci. U.S.A.* **1991**, *88*, 561−564.
(29) Lovejoy, B.; Choe, S.; Cascio, D.; McRorie, D. K.; DeGrado, W. F.; Eisenberg, D. *Science* **1993**, *259*, 1288−1293.
(30) Harbury, P. H.; Kim, P. S.; Alber, T. *Nature (London)* **1994**, *371*, 80−83.
(31) O'Shea, E. K.; Klemm, J. D.; Kim, P. S.; Alber, T. *Science* **1991**, *254*, 539−544.
(32) Hodges, R. S.; Saund, A. K.; Chong, P. C. S.; St.-Pierre, S. A.; Reid, R. E. *J. Biol. Chem.* **1981**, *256*, 1214−1224.
(33) Glatter, O.; Kratky, O. *Small-Angle X-ray Scattering*; Academic Press: London, 1982.

MA050726L